Research Paper

Volume : 3 | Issue : 7 | July 2014 • ISSN No 2277 - 8179

Computer Simulation of Luminescence in Silicon Rich Oxide thin Films Arising From Silicon-Oxygen Bonds

Computer Science

KEYWORDS : Computer Simulation, Electro-luminescence, Silicon-Rich Oxides, Chemical Bond, Density Functional Theory and Trapping-Charge Mechanism.

N. D. Espinosa-Torres	Researching Center for Semiconductor Devices, BUAP, 14 Sur y Avenida San Claudio, C. U. Edificio 103C-D, Puebla, Pue., México C.P.72570
J. F. J Flores-Gracia	Researching Center for Semiconductor Devices, BUAP, 14 Sur y Avenida San Claudio, C. U. Edificio 103C-D, Puebla, Pue., México C.P.72570
J. A. Luna-López	Researching Center for Semiconductor Devices, BUAP, 14 Sur y Avenida San Claudio, C. U. Edificio 103C-D, Puebla, Pue., México C.P.72570
D. Hernández de la Luz	Researching Center for Semiconductor Devices, BUAP, 14 Sur y Avenida San Claudio, C. U. Edificio 103C-D, Puebla, Pue., México C.P.72570
J. Martínez-Juárez	Researching Center for Semiconductor Devices, BUAP, 14 Sur y Avenida San Claudio, C. U. Edificio 103C-D, Puebla, Pue., México C.P.72570

ABSTRACT

A new Global Reaction Model (GRM)has been used to evaluate theoretically the optical properties of nanostructured Silicon-Rich Oxides (SRO) thin films. In this work we evaluate the optical spectra of a selected set of $[Si_nO_n]$ nano-structures ($5 \le n \le 26$). We obtain FTIR, Raman and luminescence spectra, besides, we calculate the Orbital Energies plots and propose a plausible mechanism for the generation of this kind of nanostructures which considers the necessary reactions for the formation of different oxide matrices along with the compositional and luminescence spectra changes, before and after the thermal treatment. For the case of luminescence studies, we make comparisons between our theoretical luminescent spectra with those of electroluminescence obtained from thin SRO films grown by the LPCVD technique, finding that the experimental observed spectrum peak at ~690 nm is in good agreement within experimental precision with the corresponding one for the calculated $Si_{15}O_{15}$ structure (694.37 nm).Similar situation happens for the case of the $Si_{11}O_{11}$ nano-structurewhich has an emission peak at 699 nm.

1.0 Introduction

Thermally treated silicon rich oxides (SRO) used as starting material for the fabrication of silicon nano dots represent the basis of tunable band gap nanostructured materials for optoelectronic and photonic applications. The optical modelization of such materials is of great interest, as it allows the simulation of FTIR, UV-Vis and Raman spectra, which are powerful non-destructive tools in the determination of phase modifications (clustering, precipitation of new phases, crystallization) upon thermal treatments.

Thin films made up of materials such as SRO, containing a tetravalent metalloid as silicon, are very relevant because they produce light emission at room temperature when are stimulated Currently, high efficiency PL as well as optical gain and light amplification have been realized in SRO thin films. Although the PL from this kind of nanostructures has achieved great progress,aversely, EL intensity generally remains too weak to allow the fabrication of efficient LED's[1].The reason for the latter to occur is mainly due to the carrier injection induced electrically and the mechanisms to generate radiative emission which are different from those induced optically. For example, the carrier injection mechanisms as well as tunneling probability in Si/SiO_2 multilayers are strongly dependent on the quantum confinement barrier height at interfaces of materials. Low carrier inyection efficiency due to the large band discontinuity between Si and silicon oxide has constrained its applications in LED´s. The SRO structure is a multi-phase material, with an excess of silicon nanocrystals (Si-nCs) or nanoclusters embedded in the oxide matrices. Oxide matrices can be silica (SiO_2), silicon monoxide (Si-O) or some sub-oxides like Si_2O_3 or Si_2O. Up tonow, the SiO_2oxide matrix has only been considered[2]. Experimentally, SRO thin films can be prepared by various techniques[4,5,6,] such as Si implantation into thermal dioxide (SiO_2), Plasma Enhanced Chemical Vapor Deposition (PECVD) and Low Pressure Chemical Vapor deposition (LPCVD). Depending on the excess of Si content, SRO exhibitsdistinctive properties such as Charge-Trapping (CT) and EL. Some novel devices have been proposed based on these outstanding properties[6,7,8].

The physical microscopic structure of SRO thin films is still a controversial subject of debate, whereby a subject of great interest to investigate is about the molecular structure and compositional details of SRO since they are very important to understand the fundamental and accurate light emission mechanisms. By this reason, in a previous work, we have already proposed and evaluated monocyclic Si_nO_{2n}structures[9], where by using DFT results we predict emission in visible region for molecular structures with less than 14 silicon atoms. Likewise, results obtained in this research predict luminescence in visible region for just about half of calculated molecular structures, especially for those with n≤16 silicon atoms, while large structures with n≥17 display luminescence in ultraviolet region.

Today, only a few models are frequently used to describe a SRO network, namely: the Mixture Model (MM) by Bell and Ley[10], the Random Bonding Model (RBM) by Philipp[11] and the Intermediate Model (IM) introduced in 2011 by Novikov and Gritsenko[12]. MM considers the SiO_x structure as a mixture of two different phases, one of which is richer in oxygen than the other. RBMdescribes the SiO_x as a single-phase structure consisting of a number of homogenously distributed randomly bonded Si-(Si_nO_{4-n}) tetrahedron with n = 0, 1, 2, 3, 4. In this case, there should not be any significant variations in the number of oxygen atoms in the vicinity of any given silicon atom, whereby the oxygen content determined by the position of the Si-O_2 stretching mode should be equal to the macroscopic oxygen content. Finally, IM assumes a smooth variation of the chemical composition at the boundaries between silicon clusters and the SiO_2 matrix, leading to a continuous distribution of the oxygen content. Relevant information was reported, in 2012, by Davor et al[13]. who, in an extensive review, considered that the actual SRO molecular structure seems to be greatly determined by the deposition procedure[14]. In order to explain the accurate molecular structure of SRO, so we find in some works that the SiOx structure films obtained by radio-frequency Sputtering[15] and physical evaporation were claimed to correspond to RBM, whereas the SiOx films obtained by magneto-sputtering[16], PECVD[17], have been assigned to MM. On the other hand, IM was used to describe SiOx layers prepared by LPCVD from SiH_4 and an N_2O source at 750 °C[12].Taking into account the foregoing models focused to study and explain correctly the actual molecular structure of SRO, in this paper we propose a new Global Reaction Model (GRM) to describe a SRO network.This model considers the global reac-

tion presents in a gas mixture of N_2O and SiH_4, annealing and secondary reactions when the SRO thin films are obtained by LPCVD technique. By using this model, we analyze a selected set of $[Si_nO_n]$ nano-structures generating their UV-Vis, FTIR and Raman spectra along with dimensions of the siliconnano-crystals. The outline of this paper is as follows: we describe the GRM in section 2, Section 3 is devoted in presenting experimental results about EL-spectra of SRO thin films obtained by LPCVD and theory about our theoretical as well as we present results of the theoretical studies of the optical properties of a variety of Si_nO_n structures presumably found in SRO thin films and conclusions.

2.0 The Global Reaction Model

In this model we consider the Global and Partial Reactions which are necessary to generate the oxide matrices (SiO_2,Si_2O_3, SiO and Si_2O), the annealing reactions for explaining the compositional changes before and after the thermal treatment and consequently the changes in spectra intensity and in a set of secondary reactions of the oxide matrices with the hydrogen produced to obtain the ions that could be associated with the emission in SRO thin films with specific defects.

2.1 Global and Partial reactions

When SRO is prepared by LPCVD, a gas mixture of N_2O and SiH_4 is habitually used[7,8]and the Si excess content can be modified by the gas flow ratio defined as Ro = $[N_2O]/[SiH_4]$. The silicon excess can be as high as 17% for Ro = 3; and the experimentally stoichiometric SiO_2 (a non-free silicon film) can be obtained for Ro ≥ 50[18]. Theoretically, Ro = 40 corresponds to the stoichiometric silica, when a silane-nitrogen mixture at 5% is used. Experimentally, there is enough evidence that SRO thin films are constituted by a silicon oxide mixture and not only by one of them, and they are independent of the value of Ro, whereby we have the global reaction given by Eq. (2.1):

$$7N_2O_{(gas)} + 114N_{2(gas)} + 6SiH_{4(gas)} - - - - \rightleftarrows (1-x)SiO_{2(solid)} + (x+y+2z+2v)Si_{solid} + (x+y+0.5*z+1.5*v)O_{2(gas)} + 12H_{2(gas)} + 121N_{2(gas)} + (1-y)SiO_{(solid)} + (1-z)Si_2O_{(solid)} + (1-v)Si_2O_{3(solid)} \quad (2.1)$$

From this,it is evident that $(SRO)_{solid}$ thin films in equilibrium are always a silicon oxide mixture constituted by the following silicon and silicon oxides quantities:

$$(1-x)\,SiO_{2(solid)}, (x+y+2z+2v)Si_{(solid)}, (1-y)\,SiO_{(solid)}, (1-z)Si_2O_{(solid)} \text{ and } (1-v)\,Si_2O_{3(solid)} \quad (2.2)$$

2.2 Annealing reactions

Depending on the silicon content excess and the post thermal treatment, both the density and size of the embedded Si-nCs can just be controlled through the deposition process, it leads that the electrical and optoelectronic properties can be improved.

When SRO thin films are annealed, some oxides are degraded. The plausible "annealing reactions" proposed are:

In these equations we point out that double arrow notation

$$SiO_{2(solid)} + Heat \rightleftarrows (1-\xi)SiO_{(solid)} + (0.5+0.5\xi)O_{2(gas)} + \xi Si_{solid} \quad (2.3)$$

$$Si_2O_{3(solid)} + Heat \rightleftarrows (1-\xi')Si_2O_{(solid)} + (2+\xi')O_{2(gas)} + 2\xi' Si_{solid} \quad (2.4)$$

stands for denoting equilibrium condition, besides, ξ and ξ'determine the progress of the annealing reactions.

With GRM is possible to predict as a consequence from reactions proposed in Eq. (2.3) and Eq.(2.4) that, after annealing, the oxides SiO and Si_2O along with Si increase in atomic composition and conversely both SiO_2 and Si_2O_3 decrease. We see that this fact agrees with RBM[11], along with data obtained experimentally[6], see Table 1.

2.3 Side-way or Secondary Reaction

Before performing the first-principles calculations, we take into account that our problem of interest must be modeled with 100 atoms at most; thereforeEq. (2.2) must be rewritten in terms of the number of atoms, leaving the following oxides:

$$Si_nO_{2n}, Si_{2n}O_{3n}, Si_nO_n, Si_{2n}O_n \quad (2.5)$$

The reactor effluent is a gaseous mixture of hydrogen, oxygen and nitrogen atoms. The produced hydrogen gas can react as follows:

$$H_2 = [H]^+ + [H:]^- \quad (2.6)$$

The formed hydrogen ion reacts with silicon oxides Eq. (2.5) and after a dehydration reaction has been carried out, it sets up the cations (see oxides in Eq.(2.7))

$$[Si_nO_{2n-1}]^{2+}, [Si_{2n}O_{3n-1}]^{2+}, [Si_nO_{n-1}]^{2+}; [Si_{2n}O_{n-1}]^{2+} \quad (2.7)$$

These oxide matrices are nanostructures with oxygen vacancies (3n-1, 2n-1 or n-1 oxygen atoms respectively). As it is widely known, Cervera et al.[19] have associated the emission in SRO thin films with specific defects, such emissions at 460 nm, 520 nm and 650 nm are related to the oxygen deficiency-related produced Centers (ODC) or oxygen vacancies.

Table 1 Oxidation states as suggested by the Random Bonding Model in SRO thin films [11] (Values as grown and annealed at 1100°C are included).

Oxidation State	Ro=30	Ro=30	Ro=20	Ro=20	Ro=10	Ro=10
Atomic %	As grown	Annealed	As grown	Annealed	As grown	Annealed
SiO_2	55.08	47.35	48.28	42.89	48.02	45.86
Si_2O_3	31.60	23.04	34.34	29.39	28.64	19.42
SiO	8.18	19.57	9.78	18.23	9.66	13.02
Si_2O	3.72	7.94	4.96	6.65	9.73	10.53
Elemental Si	1.4	2.10	2.64	2.84	3.95	11.148

Oxides described by Eq. (2.2) may react with the hydrogen in a different way forming the following anions:

The formed anions are different matrices containing oxides

$$[Si_{n-1}O_{2n(solid)}]^{4-}$$
$$[Si_{2n-1}O_{3n(solid)}]^{3-}$$
$$[Si_{n-1}O_{n(solid)}]^{2-}$$
$$[Si_{2n-1}O_{n(solid)}]^{1-}$$

with silicon vacancies or defects, and may or may not be present in the SROfilms.

3.0 Discussion of results

As is known, in the EL phenomenon, EL increases the light emission of charge carriers because electrons are injected into the conduction band and holes into the valence band, allowing band edge emissions because of the increase of probability of radiative hole-electron recombination. Additionally,EL can also be due to relaxation of charge carriers making transitions from higher energy states into radiative centers.[2]

According to experimental reports[20,21,22], EL was tested in devices having an MOS-like structure, using poly-silicon as a gate electrode (LEC, Light Emitter Capacitor). Poly-silicon is enough transparent in the emission range of SRO. On the other hand, EL in SRO, obtained by LPCVD and annealed at 1100 °C, requires applications of high electric fields and also high currents,so that these devices work at the threshold to be electrically damaged. Only devices having high photo-emission display Electroemission effects, this requirement is only found in devices with

Volume : 3 | Issue : 7 | July 2014 • ISSN No 2277 - 8179

a gas flow ratio of Ro=20 as was reported.When electrons are injected into the SRO film, the charge concentration inside the LEC distributes among the agglomeration of defects, which act as superficial and deep traps behaving as emission centers of low and high energy (red and blue centers), respectively. As has also been reported, the mobility of electrons in the SRO is very high compared with that of holes, it makes possible that the emission is attributed to electrons decaying into positive traps. Plausible emission mechanism of an LEC could be quite similar to that observed in organic light emitting diodes containing a high distribution of traps [15].

Likewise, when electrons are injected from anode into the SRO film as a consequence of applied bias voltage,a fraction of the electrons flow within the film,moving into the cathode, while the rest will be trapped by defects as already known [13], this phenomenon especially happens in SRO20 (SRO with Ro=20) films. Additionally, as the current increases, the trapped electrons,in defects, blockade the conduction paths hindering the charge carrier transport. Therefore, the higher bias voltage, the higher electron energy, so the deep traps are easier reached consequently the emitted photons are more energetic and it leads to the EL intensity is increased.

3.1Experimental Procedures

In accordance with the interest of this work for correlating the luminescence observed in SRO thin films with that calculated theoretically, here we consider firstly unpublished experimental results included in Figures (1) and (2)(provided by Morales A. et al.)*. We take luminescent spectra as a reference for comparison with regard to the wavelength values in the emitting regions that are feasible to compare with the theoretical results of our model.To obtain Electro-luminescence in LEC´s made up of SRO, obtained by LPCVD and annealed at 1100 °C, three conditions have to be satisfied: first, the density of Si_nO_n compounds in SRO thin films has to be high, second, the energy applied to the LEC has to be enough to reach the different energetic states, and third, there must be high injection of carriers from anode to produce agglomeration of electrons in the conduction trajectories in the film.From the morphological composition approach in SRO20 films, the agglomeration of defects is composed of species or molecules, which require either higher or lower energy to be excited.

Fig. 1 (color on line) Electro-luminescence spectra for SRO film with Ro=20, with applied forward-biased from 44 to 64 Volts.

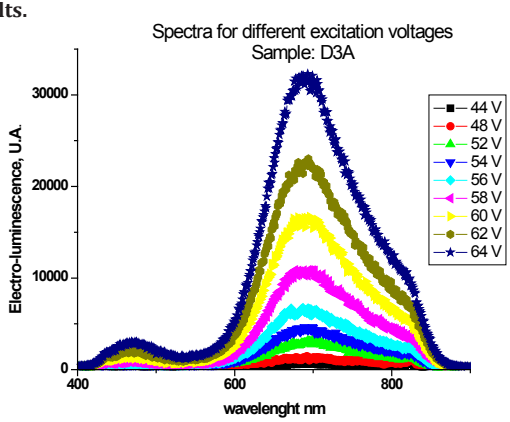

According to experimental results as shown in Figs. 1-2, by way of explanation, we have that, at low electric fields (or using UV radiation which is not this case) most of electrons will be trapped at lower energy states producing the emission mainly in the red region as indicated in Fig. 1 (forward-biased) and Figure 2 (reversed-biased).

Figure 1 displays EL spectra when SRO20 films were subjected to voltages from 44 to 64 V. The peaks intensity varies with the applied voltage and we observe that step by step each curve shows apeak which increases successively, accompanied by a secondary shifted-peak toward high energies.

From either Figure1 or Figure 2 is possible to observe an uppermost peak positioned around of 690 nm, it is similar to the one observed very frequently in PL spectrum found in literature for SRO films deposited by LPCVD.This fact is in good agreement with the theoretically calculated peak corresponding to $Si_{15}O_{15}$molecule which has an expected red emission wavelength at 694.37 nm for a triplet excited state, and could correspond with an applied voltage <50V, as well corresponds appropriately with the wavelength calculated whose values is of 699.24 nm for a $Si_{11}O_{11}$ nano-structure (see Table 7).

Fig. 2 (color on line) Electro-luminescence spectra for SRO film with Ro=20, with applied reversed-biased from -50 to -74 Volts.

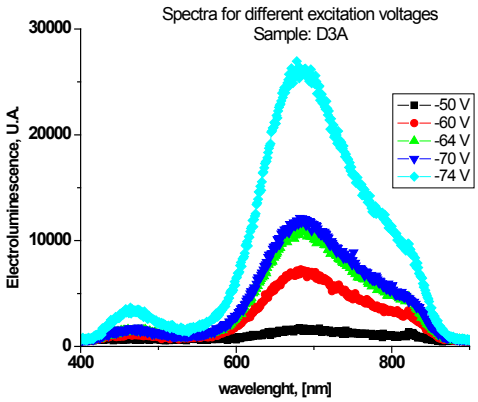

As regards the secondary blue-shift peak, when the applied energy is increased a significant density of electrons are trapped in more energetic states, so when they relax the blue emission appears with an important contribution on the radiative recombination process, besides, the higher applied reversed-biased, the higher density of electrons trapped in more energetic states consequently higher the blue-shift emission peak. This condition was theoretically found for a Si_9O_9 molecule where the calculation predicted the highest emission in blue, at 466.83 nm (review Table 7). From Fig. 2 we observe the blue-shift emission wavelength, located approximately around of675 nm. We stress that no one neutral Si_nO_n molecule with this emission wavelength was found.

3.2 Computer-GeneratedResults

In this work we employed the Density Functional Theory with the aim to evaluate theoretically the opto-electronic properties of a selected set of [Si_nO_n] nano-structures($5 \le n \le 26$). We include calculations of FTIR, Raman and luminescence spectra. Also, we compute the frontier orbitals, gaps, Mulliken atomic charges, natural charges, bond orders and geometries of all neutral molecules investigated.

3.2.1Trapping-Charge Mechanism

The interest of this work, as has been mentioned above, is to correlate experimental results with theoretical calculations based on the GRM proposed to explain the origin of the luminescence in SRO thin films. We discuss below the charge trapping mechanism and then show the results of the calculations regarding the charge distribution in molecules suggested.As a routine, the electrical properties of SRO thin films in MOS-like structures have been commonly analyzed experimentally by current versus voltage (I–V) and capacitance versus voltage (C–V) techniques. In a previous work of Morales-Sánchez et al.[2] high current was observed at low negative and positive bias voltages, but at a certain voltage (V_{drop}), the current dropped to a low conduction state until a high electric field again activated a high conduction state. C–V measurements demonstrated a capacitance reduction at the same time as the current dropped, but without appreciable flat-band voltage (V_{FB}) shifting. The drop in capacitance and current was also observed after applying an electrical stress. These effects are attributed to the annihilation of conductive paths created by Si-nCs.The conduction mecha-

nism was also analyzed by making use of theory about trap assisted tunneling and Fowler–Nordheim tunneling at low and high electric fields, respectively.Fowler–Nordheim tunneling is the wave-mechanical tunneling of an electron through an exact or rounded triangular barrier. Two types of basic situations are recognized: (1) when the electron is initially in a localized state; (2) when the electron is initially not strongly localized, and is best represented by a travelling wave. Emission from a bulk metal conduction band is a situation of the second type, and discussion here relates to this case. It is also assumed that the barrier is one-dimensional (i.e., has no lateral structure), and has no fine-scale structure that causes scattering or resonance effects. To keep this explanation of Fowler-Nordheim tunneling relatively simple, these assumptions are needed; but the atomic structure of matter is in effect being omitted. Hence, starting from the electron one-dimensional Schrödinger equation

$H\Psi(x) = E_n \Psi(x)$ rewritten as:

$$-\hat{P}\Psi = \left[U(x) - E_n\right]\Psi = M(x)\Psi$$

With $\hat{P}$ the kinetic energy operator, Ψ measured from the emitter's electrical surface [23], and $M(x)$ defined as the electron motive force which can be interpreted as the negative of the electron kinetic energy associated with the motion of a hypothetical classical point electron in the x-direction which is positive in the confinement barrier. The shape of a tunneling barrier is determined by how M(x) varies with position in the region where M(x) > 0. Two models have special status in field emission theory: the exact triangular (ET) barrier and the Schottky–Nordheim (SN) one,. For the former $M^{ET}(x) = h - eF$ M and for the latter

$$M^{SN}(x) = h - eFx - e^2/(16\pi\varepsilon_0 x)$$

here, h is the zero-field height (or unreduced height) of the barrier, e is the elementary charge, F is the barrier field, and ε0 is the vacuum dielectric constant.By convention, F is taken as positive, even though the classical electrostatic field would be negative. The SN equation uses the classical image potential energy to represent the physical effect of "correlation and exchange".This effect is modeled by using DFT for all analyzed molecules. Besides, the exchange and correlation energy may be written in terms of an average over the Coulomb-coupling-coupling constant[27],

$$E_{xc}|n| = \int_0^1 d\lambda \frac{d\langle\Psi_\lambda|V_{ee}|\Psi_\lambda\rangle}{d\lambda} - E_H, \qquad (3.1)$$

Where λ = 0 corresponds to the non-interacting case and λ = 1 to full interaction. V_{ee} is the potential electron-electron energy and EHthe hole energy.In Eq. (3.1), the density constant asλ is varied. If this is satisfied, all energy terms,except the one corresponding to the electron-electron interaction term,will remain unchanged. By the Hellman-Feynman theorem the expression in Eq. (3.1) reduces toEq.(3.2)[28],

$$E_{xc}|n| = \int_0^1 d\lambda d\left\langle\Psi_\lambda\left|\frac{V_{ee}}{d\lambda}\right|\Psi_\lambda\right\rangle - E_H \qquad (3.2)$$

The exchange and correlation energy defined in Eq. (3.2) may also be written in terms of the average exchange-correlation whole density, $\bar{n}_{xc}$ as follows

$$E_{xc}|n| = \int d\vec{r}\, d\vec{r}\,' \frac{n(\vec{r})\bar{n}_{xc}(\vec{r},\vec{r}\,')}{|\vec{r} - \vec{r}\,'|} \qquad (3.3)$$

The derivative discontinuity is a very important property in describing the gap in insulators.Table 2 lists the calculated HOMO and LUMO energies and the gap energy for $[Si_nO_n]$ molecules, where 5≤n≤26 is the number of silicon atoms in each neutral molecule studied.

An iso-surface is aconstant value (in our case the HOMO and LUMO energy) within a volume of space; in other words, it is a level set of a continuous function whose domain is 3D-space. Fig. 3 shows Iso-surface = 0.032 HOMO and Fig. 4 displays LUMO,both figures for n=16. A gray sphere represents a silicon atom and a red one an oxygen atom, whereas the bigger non spheres with blue and red color are the data mapping.

Needless to mention, neither the exchange correlation hole density nor the pair correlation function may be calculated exactly. The quality of a DFT calculation lies on how well it approximates these quantities. Many successful approximations have so far been designed making DFT a practical and powerful tool to predict several properties of many systems. While devising such approximations there are many restrictions that need to be obeyed. These all arise from the definition of the exact exchange and correlation hole energy. One of these restrictions is the derivative discontinuity: This property is very important in describing the gap in insulators. The so-called fundamental gap is defined to be the difference in energy of the same system with a number of electrons differing by one, i.e.:

$$E_g = (E_{N+1} - E_N) - (E_N - E_{N-1}) - - - (3.4)$$

Eq. (3.4) together with Koopman's theorem says that the gap energy is equal to the difference between the HOMO and LUMO-energies obtained from a Kohn-Sham calculation.

In terms of the eigenvalues, the true gap should be given as

$$E_g = \epsilon_{N+1}(N+1) - \epsilon_N(N), \qquad (3.5)$$

where what is usually available to us is the difference between HOMO and LUMO energies that we obtain in an N-electron calculation as follows,

$$\epsilon_g = \epsilon_{N+1}(N) - \epsilon_N(N). \qquad (3.6)$$

We define the following energy difference,

$$\Delta_{xc} = E_g - \epsilon_g = \epsilon_{N+1}(N+1) - \epsilon_{N+1}(N). \qquad (3.7)$$

We anticipate that the difference A_{xc} should arise from exchange and correlation contributions. By applying the variational principle together with the constraint that the density integrates to the total number of electrons, we obtain the chemical potential by the following relation:

$$\frac{\partial T_{s,M}}{\partial n} + V = \mu_M, \qquad (3.8)$$

Where M is the total number of electrons and $^1{}_M$ is the chemical potential which is the energy corresponding to the Mthorbital's eigenvalue for all M except N, T represents the kinetic energy and V the potential energy.

Table 2 HOMO; LUMO and Gap calculated using DFT, for $[Si_nO_n]$ structures, 5 ≤n≤ 26

Number of silicon atoms	HOMO eV	LUMO eV	GAP eV	Number of silicon atoms	HOMO eV	LUMO eV	GAP eV
5	-6.19	-3.14	3.05	17	-6.40	-2.47	3.93
6	-6.01	-3.46	2.55	18			
8	-5.51	-3.58	1.93	19	-6.69	-2.35	4.34
9	-5.34	-3.28	2.06	20	-6.74	-2.26	4.48
11	-5.93	-3.22	2.71	21	-6.72	-2.24	4.48
12	-5.97	-2.96	3.01	22	-6.66	-2.24	4.42
13	-5.61	-3.30	2.31	23	-6.57	-2.40	4.17
14	-6.04	-2.79	3.25	24	-6.52	-2.48	4.04
15	-6.11	-3.39	2.72	25	-6.51	-2.56	3.95
16	-6.16	-4.20	1.96	26	-6.68	-2.54	4.14

Volume : 3 | Issue : 7 | July 2014 • ISSN No 2277 - 8179

Fig. 3 Calculated HOMO Mapfor $Si_{16}O_{16}$molecule.

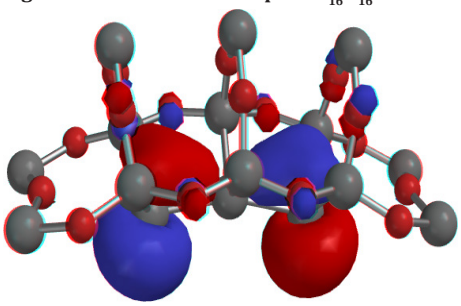

Figure 4Calculated LUMO representation for $Si_{16}O_{16}$ molecule.

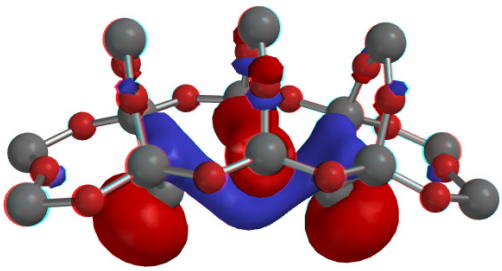

Using this approach, we evaluate the potential for structures type Si_nO_n. For example, Fig. 5 displays a slide of potential for the molecule $Si_{12}O_{12}$.Taking the difference of the two limits when M tends to N from above and to N + 1 from below we have

$$\epsilon_g = \frac{\partial T_s}{\partial \delta n_+} - \frac{\partial T_s}{\partial \delta n_-}. \qquad (3.9)$$

Thus, there is a discontinuity in the single-particle kinetic energy. Alike, such discontinuity exists in the exchange-correlation potential which is:

$$\Delta_{xc} = V_{xc}^{+} - V_{xc}^{-}, \qquad (3.10)$$

where

$$V_{xc}^{\mp} = \frac{\partial E_{xc}}{\partial n_{\mp}}. \qquad (3.11)$$

We have estimated the band gap through the evaluation of HOMO and LUMO. Besides, we have calculated others Quantitative Structure-Activity Relationships QSAR parameters with the purpose of correlate them with the size of the structures studied.

Figure 5 Calculated slide of potential for $Si_{12}On_{12}$ structure.

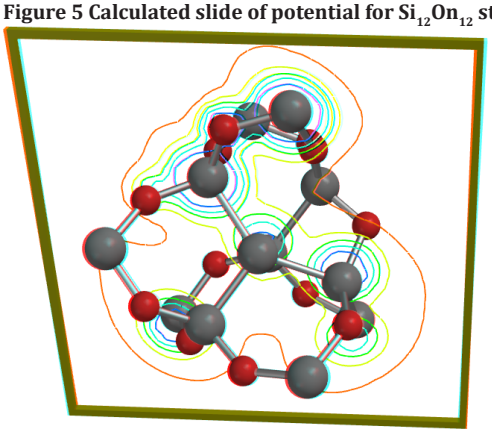

Mulliken population analysis

The luminescence phenomena in Si_nO_n structures could be focused through a trapping charge mechanism but it would be very difficult and complex to make an exhaustive theoretical calculation. Instead of that, in this work we make use of the Mulliken population analysis which permits us that the atomic charge on an atom can be calculated as the sum of the atomic orbital contributions of the atom in the occupied molecular orbital and its nuclear charge. The charge density is related to the chemical reactivity of a molecule, but being a three-dimensional function, is more convenient to define atomic charge density, which is also known as partial charge (atomic charge), approximating the complex distribution by the simplest one in which each atom has a fictive partial charge.

A density matrix is a matrix that describes a quantum system in a mixed state, a statistical ensemble of several quantum states, in contrast to a pure state, described by a single state vector. The density matrix is the quantum-mechanical analogue to a phase-space probability measure (probability distribution of position and momentum) in classical statistical mechanics. Explicitly, we suppose a quantum system may be found in state with probability ρ1, or it may be found in state $|\psi 2\rangle$with probability ρ2, or it may be found in state $|\psi 3\rangle$with probability ρ3, and so on. The density operator for this system is . $\hat{\rho} = \Sigma \rho_i |\psi_i\rangle\langle\psi_i|$Once the density matrix is determined, one can calculate many properties of the system, particularly, analyze electron density. The Mulliken population analysis, even though represents a rough partition of electronic distribution, can be easily carried out.

Integrating the expression to calculate the charge density, this integral is equal to the number of atoms N, therefore:

$$N = \sum_{\mu\nu} P_{\mu\nu} \int \phi_\nu^*(r)\phi_\mu(r)dr = \sum P_{\mu\nu} S_{\nu\mu} = \sum (PS)_{\mu\mu} = tr(PS) \qquad (3.12)$$

We see that it is then possible to assign two different ways by which many electrons are placed in each atomic orbital. The first way is that each element of the diagonal of the product is the number of electrons in the atomic orbital. It is easy to see that we thus assign effective charge per each atom if we add the number of electrons in each of the atomic orbital associated with one atom minus the positive charge of the nucleus.

$$q_A = Z_A - \sum_{\mu \in A} (PS)_{\mu\mu} \qquad (3.13)$$

This is the essence of the Mulliken population analysis. Making use of this kind of analysis, we calculate the Mulliken charge (in electron unit's |e-|) and the bonds orders (dimensionless) for the structures Si_nO_n. Particularly, for $Si_{12}O_{12}$ neutral molecule obtaining results which are shown in Fig.6, DFT was used in order to get these results.

Figure 7 displays natural charge distribution on a neutral nanostructure $[Si_{19}O_{19}]$,while in Table 3 we compare the computed values of the calculated atomic charges (Mulliken versus natural charges). In the $[Si_{19}O_{19}]$ nanostructure is possible to identify Si-Si bonds forming a penta- cycle.

Figure 6 Calculated Mulliken Charge for neutral $Si_{12}O_{12}$ molecule.

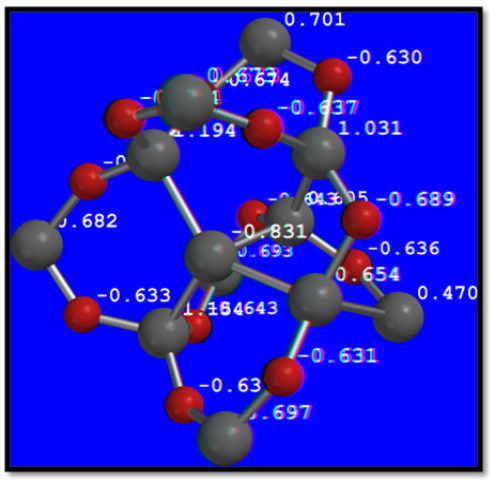

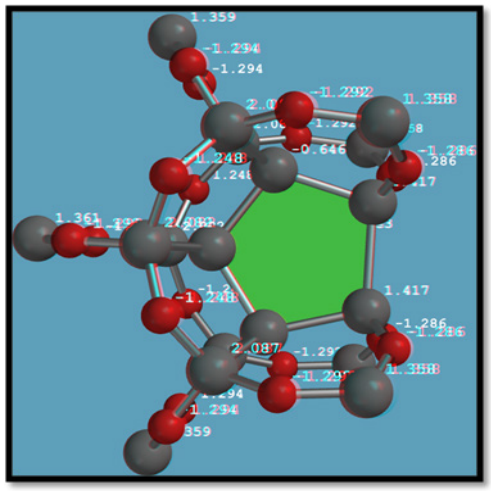

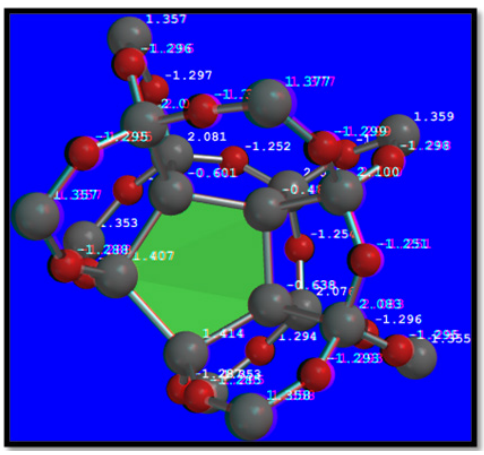

Figure 7 Calculated Natural Charges for $Si_{18}O_{18}$ (left) and $Si_{19}O_{19}$ (right).

Atom	AtomicCharges | e- |		Atom	Atomic Charges	
	Mulliken	Natural		Mulliken	Natural
Si1	+0.882	+1.417	O9	-0.646	-1.286
Si2	+0.882	+1.417	Si11	+0.686	+1.358
Si3	-0.768	-0.646	O10	-0.625	-1.292
Si4	-0.903	-0.502	Si12	+1.186	+2.087
Si5	-0.768	-0.646	O11	-0.633	-1.294
Si6	+0.686	+1.358	O12	-0.640	-1.248
O1	-0.646	-1.286	Si13	+1.298	+2.082
Si7	+1.186	+2.087	O13	-0.640	-1.248
O2	-0.640	-1.248	Si14	+1.186	+2.087
Si8	+1.298	+2.082	O14	-0.625	-1.292
O3	-0.640	-1.248	O15	-0.646	-1.286
Si9	+1.186	+2.087	Si15	+0.686	+1.358
O4	-0.633	-1.294	O16	-0.633	-1.294
O5	-0.641	-1.292	Si16	+0.685	+1.359
O6	-0.625	-1.292	O17	-0.641	-1.292
O7	-0.625	-1.292	Si17	+0.682	+1.361
Si10	+0.686	+1.358	O18	-0.633	-1.294
O8	-0.646	-1.286	Si18	+0.685	+1.359

Table 3 Atomic Charges calculated (Mulliken versus Natural charges) for a [$Si_{18}O_{18}$] neutral nanostructure.

Additionally, the red highlighted cells, in Table 3, show the four silicon atoms with a Mulliken charge of 1.186 (corresponding to Si_7, Si_9, Si_{12} and Si_{14}). It is noteworthy that silicon atoms identified as Si_8 and Si_{13}both exhibit the highest Mulliken atomic charges (+1.298).

The absolute values of the Mulliken charges in the remaining 12 silicon atoms, in this molecule, are less than unity, from whichnine have positive charges and three negative ones. The silicon atoms identified as Si_2, Si_3 and Si_4 forming part of a penta-cycle constituted exclusively of silicon atoms are those that exhibit this unusual behavior in Mulliken charge.

Atom1	Atom2	Bond Order	Atom1	Atom2	Bond Order	Atom1	Atom2	Bond Order	Atom1	Atom2	Bond Order
Si1	Si2	0.796	Si6	O6	0.928	Si4	O2	0.039	Si11	O10	0.928
Si1	Si5	0.784	Si7	O2	0.961	Si4	Si8	0.818	Si11	Si12	0.077
Si1	Si10	0.073	Si7	Si8	0.076	Si4	O3	0.039	O10	Si12	0.972
Si1	O8	0.908	Si7	O6	0.972	Si4	Si9	0.040	Si12	O12	0.961
Si1	O15	0.908	Si7	O11	0.952	Si4	O5	0.057	Si12	Si13	0.076
Si1	Si15	0.073	Si7	Si16	0.077	Si4	Si12	0.039	Si12	O16	0.952
Si2	Si3	0.784	O2	Si8	0.961	O16	Si16	0.929	Si12	Si16	0.077
Si2	Si6	0.073	Si8	O3	0.961	Si4	O12	0.039	O11	Si16	0.929
Si2	O1	0.908	Si8	Si9	0.076	Si4	Si13	0.818	O12	Si13	0.961
Si2	O9	0.908	Si8	O5	0.959	Si4	O13	0.039	Si13	O13	0.961
Si2	Si11	0.073	Si8	Si17	0.079	Si4	Si14	0.040	Si13	Si14	0.076
Si3	Si4	0.851	O3	Si9	0.961	Si4	O17	0.057	Si13	O17	0.959
Si3	O1	0.064	Si9	O4	0.952	Si5	Si9	0.837	Si13	Si17	0.079
Si3	Si7	0.837	O17	Si17	0.930	Si5	O4	0.067	O13	Si14	0.961
Si3	O6	0.061	Si9	O7	0.972	Si5	O7	0.061	Si14	O14	0.972
Si3	O9	0.064	Si9	Si10	0.077	Si5	O8	0.064	Si14	Si15	0.077
Si3	O10	0.061	Si9	Si18	0.077	Si5	Si14	0.837	Si14	O18	0.952
Si3	Si12	0.837	O4	Si18	0.929	Si5	O14	0.061	Si14	Si18	0.077
Si3	O11	0.067	O5	Si17	0.930	Si5	O15	0.064	O14	Si15	0.928
Si3	O16	0.067	O7	Si10	0.928	Si5	O18	0.067	O15	Si15	0.926
Si4	Si5	0.851	Si10	O8	0.926	Si6	O1	0.926	O18	Si18	0.929
Si4	Si7	0.039	O9	Si11	0.926	Si6	Si7	0.077			

Table 4 Bond Order Mulliken for a[$Si_{18}O_{18}$] neutral molecule.

Volume : 3 | Issue : 7 | July 2014 • ISSN No 2277 - 8179

Table 4 lists Mulliken bond orders (dimensionless) for a $Si_{18}O_{18}$ nano-structure. In this Table we point out with blue highlighted cells some bond orders Si-Si which exhibit weak bonds of around of 0.07 or 0.04, e.g., Si_1-Si_{10}, Si_1-Si_{15}, Si_2-Si_{11} and so on. These silicon atoms are joined to each other through oxygen atoms.

We identify, besides, a penta-cycle forming a green highlighted plane in Fig. 7. The red highlighted cells in Table 4 mark out some representative silicon atoms which are strongly joined. Si_1-Si_5, Si_1-Si_2, Si_3-Si_4 (Mulliken's bond order varies from 0.784 to 0.851).

3.2.2 Calculated Fourier Transform Infra-red Spectroscopy (FTIR) and Raman spectra

In this work we are interested in studying the normal modes of vibration of the Si_nO_n structures for which we make use of DFT in order to compute the Hessian matrix and obtain the FTIR and Raman spectra.

This Hessian matrix contains the second derivatives of the molecular energy (measured with a method of electronic structure) with respect to the molecular coordinates. By diagonalizing this matrix we obtain: (1) the normal modes of vibration which are combinations of the atomic coordinates, they allow an easy description of the vibrational motion of the molecule, because the potential energy associated with the vibrational modes can be decomposed as the sum of harmonic terms, one for each normal mode, (2)the vibrational frequencies associated with each normal mode which can be assigned to the frequencies observed in the IR and Raman spectra.

A systemic theoretical study was done recently by Zhan[16] and Shu-Xian Hu et al.[31] on the structural and electronic properties of ground-state silicon monoxide clusters $(SiO)_n$, $1 \le n \le 26$.

For our case of interest, we apply DFT in order to calculate FTIR and Raman spectra for $[Si_nO_n]$ neutral nanostructures, $5 \le n \le 26$ excluding n=18, because we have convergence troubles, and n=7, 10 because suchstructures are either inexistent or currently unknown. Fig. 8 displays the FTIR spectrum calculated for one of the simplest Si-O structures considered. This molecular structure is constituted by five silicon atoms and five oxygen atoms, and they form two rings of three silicon atoms each one. These rings are linked by a silicon atom and placed in orthogonal planes.

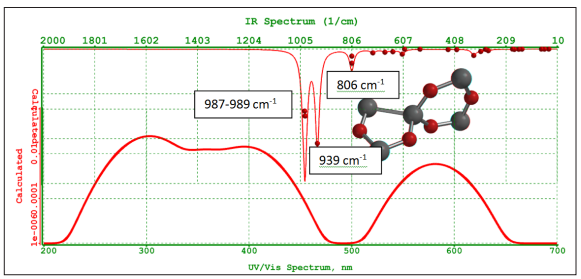

Figure 8 $[Si_5O_5]$ molecular structure formed by two rings placed in orthogonal planes joined by a silicon atom and the corresponding calculated FTIR spectrum (top) and Uv-Vis spectra (bottom)

We identify three outstanding peaks associated with vibrational frequencies located at 987-989 cm_{-1} (the uppermost peak) overlapped with intensities of 746.87 and 691.98 arbitrary units (A.U.), besides at 939 cm^{-1} (the middle peak) with 1053.66 U.A. and lastly at 806 cm^{-1} (the lower peak), besides, the lowest peaks with 157.39 A.U. overlapped with a small vibration of 78.99 U.A. at the same frequency. In figure the filled circles situate the positions of intensity for each peak. The uppermost and middle peaks both are due to stretching mode Si-O bonds whereas the lower peak corresponds to stretching mode Si-O bonds in cycle that includes a Si-Si bond (see Fig. 8). The two furthest small peaks are associated with rocking mode vibrations in Si-O bonds each one in each cycle.

Siliconatoms in [Si11O11]		Distance calculated Å
Si7	Si2	5.271
Si2	Si8	3.754
Si2	Si3	3.725
Si3	Si8	3.755
Si2	Si6	3.67
Si8	Si6	3.531
Si6	Si3	3.672
Si3	Si7	5.279
Si7	Si8	2.559
Si7	Si6	3.166

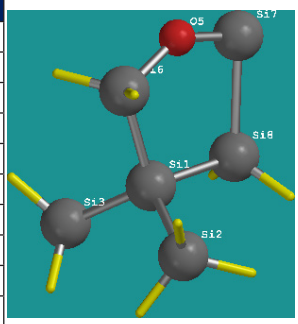

Table 5 Dimensions calculated corresponding to a silicon nano-crystal embedded in a $[Si_{11}O_{11}]$ molecule.

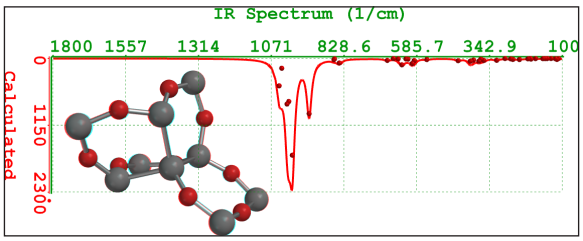

Figure 9 The FTIRspectrum calculated for $[Si_9O_9]$ molecular structure which consists of four cycles of which three containSi-Si-Si bonds and the other only a Si-Si bond. Because of the superposition of the rings, it is only possible to identify clearly three of them.

As regards Si_5O_5 molecule it exhibits photo luminescence both in ultraviolet region (at 303.26 nm) and in visible region (at 581.52 nm). The calculated emission intensity is similar in both regions; refer to Figure 8 (bottom).

On the other hand, it is found that as the agglomerate size is increased, the number of mini-rings formed increasesas well. To corroborate this fact, we analyze the Si_9O_9 molecular structure. This is shown in Figure 9 along with its FTIR spectrum. This nanostructure consists of four cycles eachone includes four silicon atoms. Three of them contain Si-Si-Si bonds and the other cycle has only a Si-Si bond. The FTIR spectrum exhibits the highest peak, constituted by five vibrational frequencies (filled circles), and located in the interval of 1001 to 1045 cm^{-1}. Every one of the four cycles generates a specific stretching mode vibration due to Si-O bonds in the cycle, besides, the Si-O bond in cycle together with Si-Si one gives rise to an additional stretching mode.

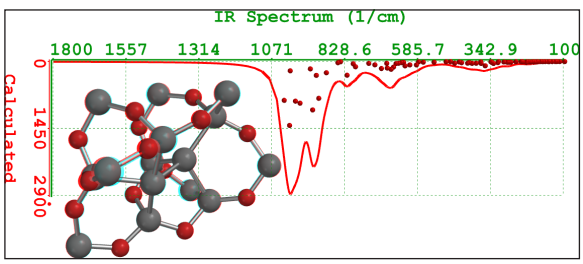

Figure 10 Structure and FTIR calculated for $[Si_{15}O_{15}]$

Figure 10 shows a more complicated molecular structure. It corresponds to the $Si_{15}O_{15}$ nano-agglomerate which is constituted of 7 mini-rings. Six of them have Si-Si-Si bonds and the last ring has four joined silicon atoms, that is, the Si-Si-Si-Si chain. Additionally it is possible to form a longer ring without Si-Si bonds (with only Si-O bonds). In this case the FTIR spectrum exhibits mainly five peaks. From the Figure 10, we see that the most intense peaks correspond to frequencies ranking from 993 to 1030 cm_{-1}.

The middle size peak includes overlapped frequencies varying from 889 cm^{-1} to 977 cm^{-1}. The remaining small peaks have definite frequencies at 820, 665 and 360 cm^{-1}. The corresponding calculated UV-Vis spectrum (not reported) predicts emission in visible region in two regions one of them with two intervals varying from 412.98 to 429.86 nm, and the other from 444.77 to 451.43 nm and the other region with the corresponding wavelengths varying from 546.22 to 694.37 nm respectively.

Figure 11 shows the molecular structure of the $Si_{20}O_{20}$agglomerate along with its FTIR spectrum. In this case a penta-cycle of silicon atoms is formed, and is green highlighted analogous to that obtained for the case of the $Si_{19}O_{19}$structure shown in Fig. 7 above, but it is noteworthy that in this case four silicon atoms are approximately located on the same plane and the other silicon atom forms a dihedral angle of -9.69°. The FTIR spectrum calculated for the $Si_{20}O_{20}$agglomerate is quite similar to one obtained for the agglomerate of fifteen silicon atoms. Additionally there is a small shoulder to the left-side of the utmost peak with a frequency of about 1081 cm^{-1}. This noticeable small shoulder not only persists but also shifts for greater agglomerates, such that found in the $Si_{26}O_{26}$ molecule at the vibration frequency of about 1101cm^{-1} (refer to Fig. 12).

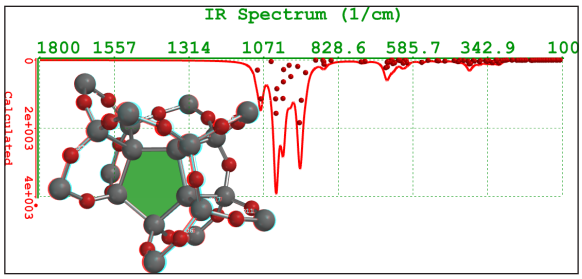

Figure11FTIR spectrum calculated for $[Si_{20}O_{20}]$

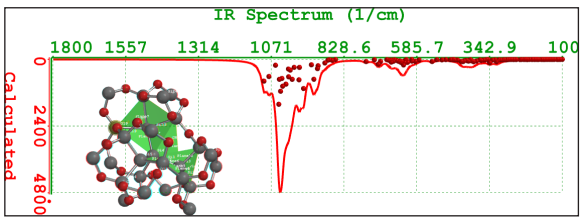

Figure 12FTIR spectrum calculated for the$[Si_{26}O_{26}]$ structure.

In this case the silicon penta-cycle which is formed in smaller structures is transformed into a pyramid, and the stress on central silicon atom is strongly increased, it yields this structure emits only in ultraviolet region.

Figure 13 displays calculated Raman spectra for the $[Si_{11}O_{11}]$ molecular structure. It forms a nanostructure with five Si-Si bonds formed with six silicon atoms (i.e., Si_1, Si_2, Si_3, Si_6, Si_7 and Si_8). According to the optical phonon confinement effect in low dimensional structures, the size of silicon nanocrystals can be estimated from both the position and width of the peak localized around of 521 cm^{-1} following the analysis of Campbell and Fauchet[32]. In agreement with Sony[33] reports as the size of embedded silicon nanocrystals in silica decreases from 2.2 to 1.4 nm, the Raman peak shifts from 511 to 502 cm^{-1}.

We identify in Raman spectrum, displayed in Fig. 13, a small peak at 490 cm^{-1} likewise at 487 cm^{-1} in Figure 14. Those vibrational frequencies correspond to Si-Si bonds for sizes 0.38 to 0.51 nm which, in turn, corresponds to the values of the average distance calculated from data in Table 5 and Table 6).

Silicon atoms in $[Si_{22}O_{22}]$		Distance calculated Å
Si1	Si2	2.353
Si1	Si13	5.675
Si1	Si8	5.537
Si1	Si12	5.543
Si1	Si7	5.208
Si2	Si14	5.545
Si2	Si9	5.279
Si2	Si8	5.676
Si2	Si13	5.535

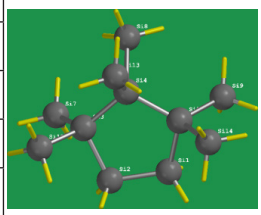

Table 6 Dimensions calculated for a silicon nano-crystal embedded in a $[Si_{22}O_{22}]$ molecule.

Considering the results obtained in this research, it is possible to fit with the Eq. (3.14) the calculated vibrational frequencies in the molecular structures Si_n-O_n, due to silicon nanocrystals versus the number of silicon atoms by the following relation:

$$\nu = 37.095\ ln(NSAN) + 375.54 \qquad (3.14)$$

Where ν is the Raman vibrational frequency in cm^{-1} and NSAN is the number of silicon atoms in nanostructures type Si_nO_n.[32] This equation reproduces the experimental vibrational frequency data in structures with Si-O bonds, published by Sony [33] and Fauchet[32], satisfactorily.

As has been done previously we calculated the Si-Si bonds lengths for the $[Si_{11}O_{11}]$ moleculeobtaining their values ranging from 2.2479 to 2.5587 Å, the prominent dimensions of nanocrystal formed are calculated and listed in Table 5.We stress that in the $[Si_{11}O_{11}]$molecule, four silicon atoms form a tetragonal pyramid, Si_1 is located in the center of the crystal, and Si_7 is joined to the pyramid directly to Si_8 and through the oxygen atom O_5 to the silicon atom Si_6.

Figure 14 displays calculated Raman spectra for the $[Si_{22}O_{22}]$ structure, this latter consists of a nano-structure with eleven Si-Si bonds formed with eleven silicon atoms (Si_1, Si_2, Si_3, Si_4, Si_5, Si_7, Si_{12}, Si_8, Si_{13}, Si_9 and Si_{14}). In this molecule, silicon nano-crystal embedded in $Si_{22}O_{22}$ forms a cycle of fivesilicon atoms and additionally three silicon atoms in cycle have joined two silicon atoms each one.

For the $Si_{22}O_{22}$molecule, calculated Si-Si bond lengths are in an interval from 2.3534 to 2.3971Å. Dimensions of crystals embedded in a $Si_{22}O_{22}$molecule are displayed in Table 6.

Considering the results obtained in this work, we report that the number of Si-Si bonds in neutral structures type $[Si_nO_n]$is well built-in by Eq. (3.15)with a correlation factor R^2 equal to 0.982.

$$\text{Number of Si} - \text{Si bonds} = 1.053(n)^{0.897} \qquad (3.15)$$

Where $5 \leq n \leq 26$ is the number of silicon atoms in the molecular structure.

Nevertheless, the number of Si-Si bonds is an integer number (not a real number), and in consequence, for the structures investigated takes only the following values: {1, 2, 3, 5, 6, 8, 11 and 14}.

Volume : 3 | Issue : 7 | July 2014 • ISSN No 2277 - 8179

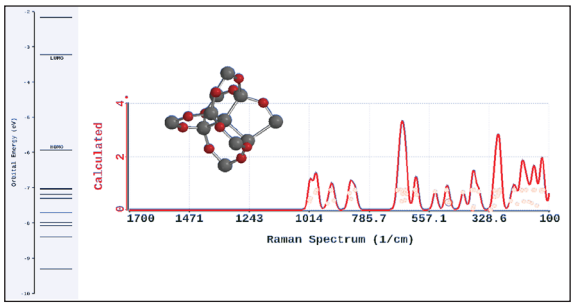

Figure 13 Calculated Raman spectra for [$Si_{11}O_{11}$]. In the center of the figure is the atomic structure and the left side inset displays the Orbital Energy (eV)

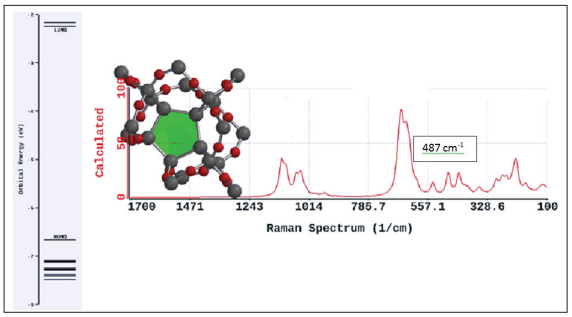

Figure 14 Calculated Raman spectra for [$Si_{22}O_{22}$]. In the center of the figure is the atomic structure and left inset displaysthe Orbital Energy (eV).

3.2.3 Calculated Luminescence Spectra of Neutral Si_nO_n molecules

Average dimensions of silicon nano-crystals embedded in $Si_{11}O_{11}$ molecule (~3.7 Å) are smaller than the average ones of nano-crystals in the $Si_{22}O_{22}$molecule (~5.5Å).

Now, we focus on the UV-Vis spectra calculated for the $Si_{11}O_{11}$ molecule, they predict, on one hand, emission in the ultraviolet region at 377.58 nm and, on the other hand, emission in visible region at 699.24 nm (red), whilst for the $Si_{22}O_{22}$ molecule, our results predict only one emission peak at 310.16 nm (ultraviolet region), see Figure 15.

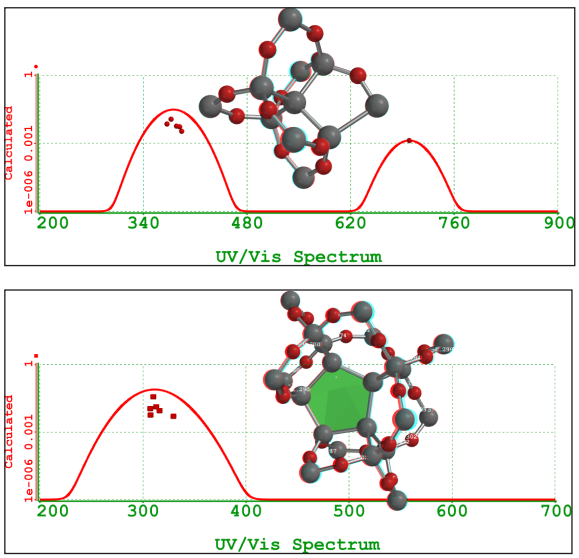

Fig. 15 The UV-Vis spectrum for the $Si_{11}O_{11}$structure (top plot) and the UV-Vis spectrum for the $Si_{22}O_{22}$ (bottom plot).

In this paper, we make use DFT for evaluating the UV-Vis spectra for [Si_nO_n] structures, where we identify *n* as the number of silicon atoms. The UV/Vis spectra are carried out by means of the TD-DFT calculation after the main wavefunction has been calculated.In Configuration interaction based on single-electron promotions only(the so-called CIS method) the absorption energies are the difference between the energies of the Hartree-Fock (HF) ground state and the CIS excited state[34]. The electronic states of most molecules can be divided into singlet states and triplet states.

The singlet states take place when all electrons in the molecule are spin-paired and the triplet states when one set of electron spins is unpaired. In Table 7, we have listed results for wavelengths of emission calculated in visible and ultraviolet regions for Si_nO_n (structures for molecules with $n \geq 12$ silicon atoms). Into the software employed, we have chosen options in order to evaluate the triplet states. The intensity of these excitations will be small (zero) but can be useful if we are interested in all lower energy excited states.

Number of silicon atoms	Wavelength of maximum emission in visible region, nm.	Wavelength of maximum emission in Ultra violet region, nm.	Number of silicon atoms	Wavelength of maximum emission in visible region, nm.	Wavelength of maximum emission in Ultra violet region, nm.
5	581.52	303.26	17	none	335.96
6	772.80	373.12	18		
8	534.57	none	19	none	321.32
9	466.83	none	20		313.58
11	699.24	377.58	21		310.30
12	495.20 (max) Triplet at 430.62-444,65 and 580.34	none	22	none	310.16
13	485.26 (max), doublets at 435.69-451.28 and509.46-740.88	none	23	none	342.60
14	444.45	371.17	24	none	328.89
15	Triplet at 444.77-451.43 and 694.37	none	25	none	325.64
16	497.63 (max) Doublet at 549.80-556.00	none	26	none	329.95

Table 7 Wavelengths of emission calculated in visible and ultraviolet regions for Si_nO_n structures.

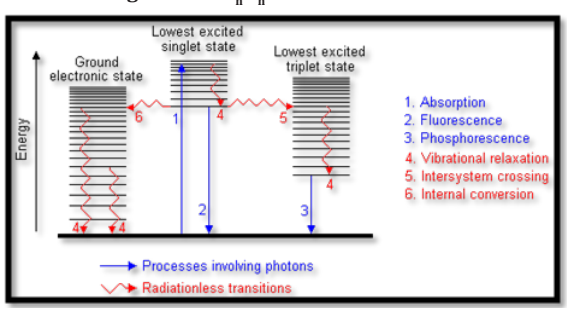

Figure 16 Possible physical process following absorption of a photon by a molecule

Absorption of UV radiation by a molecule excites it from a vibrational level in the electronic ground state to one of the many vibrational levels in the electronic excited state. This excited state is usually the first excited singlet state. A molecule in a high vibrational level of the excited state will quickly fall to the lowest

vibrational level of this same state by losing energy where this lost energy is transferred to other molecules through collisions. The molecule will also partition the excess energy by other possible modes such as vibrations and rotations. For example, Fluorescence occurs when the molecule returns to the electronic ground state, from the excited singlet state, by emission of a photon. However, if this molecule does not fluoresce it means that it must have lost its energy by some other way. This process is called radiationless transfer of energy (see Figure 16). On the other hand, a molecule in the excited triplet state may not always use intersystem crossing to return to the ground state. It could lose energy by emission of a photon.

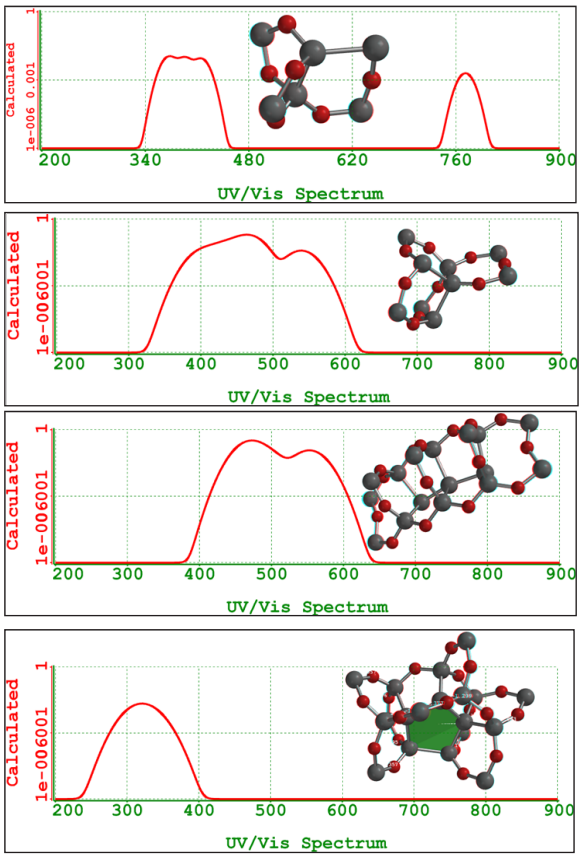

Fig.17 Luminescence spectra calculated for neutral nanostructures top to down (a) [Si_6O_6], (b) [Si9O9], (c) [Si16O16] and (d) [Si19O19].

We point out thata triplet/singlet transition is much less probable than a singlet/singlet one. The lifetime of the excited triplet state can be up to 10 seconds, in comparison with 10^{-5} s to 10^{-8} s average lifetime of an excited singlet state. Emission from triplet/singlet transitions can continue after initial irradiation. Internal conversion and other radiationless transfer of energy compete so successfully with phosphorescence in such an extent that it is usually seen only at low temperatures or in highly viscous media.

For DFT calculations, excited states are obtained using time dependent DFT calculations[35,36]. Our results predict luminescence in visible region for approximately half of the calculated structures, specifically for $n \leq 16$ silicon atoms, and large structures with $n \geq 17$ exhibit luminescence in ultraviolet region. We display in Figure 17 (a) to (d) some of the calculated UV-Vis spectra and their structures.

4.0 Conclusions

In this report we have employed DFT for evaluating theoretically the structures Si_nO_n type structures, where $5 \leq n \leq 26$ is the number of silicon atoms in such structures, additionally, it has been introduced a new GRM model as a novel approach to explainthe physical microscopic structure of the SRO thin films.

This model firstly considers the compulsory Global and Partial Reaction(s) to produce the oxide matrices (identified as SiO_2, Si_2O_3, SiO and Si_2O), secondly the annealing reactions for elucidating the compositional changes before and after the thermal treatment and subsequently the variations in the intensity of luminescence spectra, furthermore, it describes a set of secondary reactions of the oxide matrices with the hydrogen produced in the reaction chamber to obtain the charged species that could be associated to the emission in the SRO thin films with explicit defects. We point out that in this work we only evaluate the SiO type oxides matrices as suggested by Shu-Xian Huet al.[31].

On the other hand, the information obtained from the calculated Raman spectra has permitted us to establish an analytical expression for the vibrational frequencies in theoretically calculated Si_n-O nmolecules, due to silicon nanocrystals versus number of silicon atoms. Along with these important results, we have computed the dimensions of silicon agglomerates in the SiO type oxide matrix. Taking into account this information we were able to make comparisons with crystallographic experimental data of the SRO films.

Finally, in the case of the forward-biased SRO obtained by the LPCVD technique, with Ro=20 (SRO20 structure) whose Electro-Luminescence experimental results are known as reported in literature, we compared these results with those ones obtained from our theoretical calculations resulting from this that the observed experimental spectrum peak at ~690 nm is in good agreement with the calculated $Si_{15}O_{15}$ molecule spectrum peak obtained in theoretical PL studies which presents an expected red emission at approximately 695 nm for a triplet excited state, and it could correspond with an applied voltage <50V. Also, this corresponds suitably with the calculated wavelength of 699 nm for a $Si_{11}O_{11}$ nano-structure.

Acknowledgments

N.D. Espinosa-Torres acknowledges the financial support of CONACYT for the grant to carry out Ph.D. studies and the facilities given by ICUAP,and CIDS-BUAP.We acknowledge the partial financial supports of CONACyT and VIEP-BUAP through projects CB-CONACyT-2010-01-154725 and LULJ-EX_C12-I.

REFERENCE

[1]Xiang W, Rui H, Chao S, Yanqing G, Jie S, Effect of barrier layers on electroluminescence from Si/SiOxNy multilayer structures, App PhysLett 102:081114. (2013). | [2]Morales-Sánchez A, Barreto J, Dominguez C, Aceves M, Luna-López JA, The mechanism of electrical annihilation of conductive paths and charge trapping in silicon-rich oxides. Nanotechnology 20:4. (2009). | [3]Shimizu-Iwayama T, Kurumado N, Hole DE, Townsend PD, Optical properties of silicon nanoclusters fabricated by ion implantation, J ApplPhys 83:6018–22. (1998). | [4]Dusane S, Bhave T, Hullavard S, Bhoraskar SV, Lokhare S, Electron exo-emission study of PECVD and thermal CVD silicon rich silicon oxide. Solid State Commun 111:431–5. (1999). | [5]Calleja W, Falcony C, Torres A, Aceves M, Osorio R, Optical properties of non-stoichiometric SiO2 as a function of excess silicon content and thermal treatments, Thin Solid Films 270:114–7. (1995). | [6]Calleja W, Aceves M, Falcony C EEPROM transistor fabricated with stacked SiOx LPCVD films. Electron Lett 34:. (1998) 1294–1296. | [7]DiMaria DJ, Dong DW, Pesavento FL, Enhanced conduction and minimized charge trapping in electr-ically alterable read-only memories using off-stoichiometric silicon dioxide films, J ApplPhys 55:. (1984) 3000–3019. | [8]Aceves M, Carrillo J, Carranza J, Calleja W, Falcony C, Rosales P, Duality metal oxide semiconductor-PN junction in the Al/silicon rich oxide/Si structure as a radiation sensor, Thin Solid Films 373: (2000) 134–136. | [9]Aceves M, Espinosa-Torres ND, Flores-Gracia F, González-Fernández AA, López-Estopier R, Román-López S, Pedraza G, Domínguez C, Morales A, Falcony C, Composition and emission characterization and computational simulation of silicon rich oxide films obtained by LPCVD, Surf Interface Anal Special issue article Published online in Wiley Online Library. (wileyonlinelibrary.com) DOI 10.1002/sia.5212. (2013). | [10]Bell FG, Ley L, Photoemission study of SiOx (0 < x < 2) alloys, Phys Rev B 37: (1988) 8383-9393. | [11]Philipp HR, Optical properties of non-crystalline Si, SiO, SiOx and SiO2, J PhysChem Solids 32(8): (1971) 1935–1945. | [12]Novikov YuN, Gritsenko VA, Short-range order in amorphous SiOx by x ray photoelectron spectros-copy, J ApplPhys 110:014107. (2011). | [13]Davor R, Mile I, Giorgio S, Zdravko S, Bogdanović-Radović I, Marijan M, Mira R, Ozren G, Sveto-zar M, Krešimir F, Giancarlo CR, Maurizio F, Local site distribution of oxygen in silicon-rich oxide thin films: A tool to investigate phase separation, J PhysChem C 116: (2012) 10039–10047. | [14]Durrani SMA, Al-Kuhaili M F, Khawaja E, Characterization of thin films of a-SiOx (1.1<x<2.0) pre-pared by reactive evaporation of SiO, J PhysCondens Matter 15: (2003) 8123-8135. | [15]Shabalov AL, Feldman MS, Optical properties and structure of thin SiOxfilms, Thin Solid Films 151:317. (1987). | [16]Zhang WL, Zhang S, Yang M, Chen TP, Microstructure of Magnetron Sputtered Amorphous SiOx Films: Formation of Amorphous Si Core-Shell Nanoclusters. J PhysChem C 114 : (2010) 2414-2420. | [17]Hui-Dong Y, Zhong-Yi S, The role of hydrogen in hydrogenated micro-crystalline silicon film and in deposition process with VHF-PECVD technique, Chinese Phys 15:1374. (2006). | [18]Dong D, Irene EA, Preparation and some properties of CVD Si-rich and Si3N4 films, Solid-state sci and tech J Electrochem Soc 125: (1978) 819–823. | [19]Cervera M, Hernández MJ, Rodríguez P, Piqueras J, Avella M, González MA, Blue-cathodoluminescent layers synthesis by high-dose N+, C+ and B+ SiO2 implantation, Journal of Lumi-nescence 03; 117(1): (2006) 95–100. DOI:10.1016/j. jlumin.2005.03.015. | [20]González-Fernández AA, Aceves-Mijares M, Morales Sánchez A, Leyva KM, Intense whole area electro luminescence from low pressure chemical vapor deposition-silicon-rich oxide based light emit-ting capacitors, J ApplPhys 108:043105. (2010). | [21]Aceves-Mijares M, González-Fernández AA, López-Estopier R, Luna A, Berman-Mendoza D, Mo-rales A, Falcony C, Domínguez C, Murphy R, Hindawi Publishing Corporation, Journal of Nanomate-rials, Volume 2012, Article ID 890701, 11 pages, doi:10.1155/2012/ 890701(2012). | [22]Zhenrui Y, Aceves M, Carrillo J, Flores F, Single electron charging in Si nanocrystals embedded in silicon rich oxide, Nanotechnology 14: (2003) 959–964. | [23]Forbes R, The electrical surface as centroid of the surface-induced charge, Ultra microscopy 79: 25. doi:10.1016/S0304-3991(99)00098-4. (1999). | [24]Herring C, Nichols M, Thermo ionic Emission, Rev. Modern Phys. 21(2):185. doi:10.1103/Rev Mod Phys.21.185. (1949). | [25]W. Schottky, Überden Einfluβ von Strukturwirkungen, besonders der Thom-sonschenBildkraf, auf dieElecktronenenmission der Metalle. PhysZeitschr 15:872. (1914). | [26]Nordheim LW, The Effect of the Image Force on the Emission and Reflexion of Electrons by Metals, Proc. Royal Soc. Lond. A 121(788):626. (1928). | [27]H. Toffoli,NanoDFT School - IYTE 2009, Izmir Institute of technology. | http://nanodft09.iyte.edu.tr/pdf/HT-L2.pdf | [28]J. Hafner, Foundation of Density Functional Theory, InstitutfurMaterialphysicandCenterforComputa-tionalMaterialScienceUniversitatWien,Sensengasse8/12,A-1090Wien,Austria. http://www.vasp.at/vasp-workshop/slides/dft_introd.pdf | [29]Koopmans, Tjalling (1934). "Über die Zuordnung von WellenfunktionenundEigenwertenzu den ein-zelnenElektroneneinesAtoms". Physica (Elsevier) 1 (1–6): 104–113. Bibcode:1934Phy.....1..104K. doi:10.1016/S0031-8914(34)90011-2 | [30]Andrés JM, Bertrán J, Theoretical and ComputationalChemistry: Foundations, Methods and Techni-ques, Eds., Publicaciones de la U. Jaume I, Castellón de la Plana, 2007. | [31]Shu-Xian H, Jian-Guo Y, Eddy YZ, A Density Functional Study of the Structural and Electronic Properties of Silicon Monoxide Clusters, J. Phys. Chem. A 114: (2010)10769–10774. | [32]Campbell IH, Fauchet PM, The effects of microcrystal size and shape on the one phonon Raman spectra of crystalline semiconductors, Solid State Communications, 58, Issue 10: (1986) 739-741. | [33]Soni RK, Fonseca LF, Resto O, Buzaianu M, Weisz SZ, Size-dependent optical properties of silicon nanocrystals. Journal of Luminescence 83-84: (1999) 187-191. | [34]Foresman JB, Head-Gordon M, Pople JA, Frisch MJ, Toward a Systematic Molecular Orbital Theory for Excited States. J PhysChem (1992) 96:135. | [35]Runge E, Gross EKU, Density-functional theory for time-dependent systems.Phys Rev Lett 52: (1984) 997-1000. | [36]Hirata S, Head-Gordon M, Time-Dependent Density Functional Theory within the Tamm-Dancoff Approximation, Chem. Phys. Lett. 314:(1999).291-299. |